

Weakly supervised image segmentation for defect-based grading of fresh produce

Manuel Knott^{a,b,c}, Divinefavour Odion^d, Sameer Sontakke^e, Anup Karwa^e, Thijs Defraeye^{a,*}

^a*Empa, Swiss Federal Laboratories for Materials Science and Technology, Laboratory for Biomimetic Membranes and Textiles, St. Gallen, Switzerland*

^b*Swiss Data Science Center, ETH Zurich and EPFL, Zurich, Switzerland*

^c*Institute for Machine Learning, Department of Computer Science, ETH Zurich, Switzerland*

^d*Constructor University Bremen, Campus Ring 1, 28759, Bremen, Germany*

^e*Innoterra BioScience Private Limited, Mumbai, India*

Abstract

Implementing image-based machine learning in agriculture is often limited by scarce data and annotations, making it hard to achieve high-quality model predictions. This study tackles the issue of postharvest quality assessment of bananas in decentralized supply chains. We propose a method to detect and segment surface defects in banana images using panoptic segmentation to quantify defect size and number. Instead of time-consuming pixel-level annotations, we use weak supervision with coarse labels. A dataset of 476 smartphone images of bananas was collected under real-world field conditions and annotated for bruises and scars. Using the Segment Anything Model (SAM), a recently published foundation model for image segmentation, we generated dense annotations from coarse bounding boxes to train a segmentation model, significantly reducing manual effort while achieving a panoptic quality score of 77.6%. This demonstrates SAM's potential for low-effort, accurate segmentation in agricultural settings with limited data.

Keywords: Machine Learning, Computer Vision, Food Quality, Postharvest

1. Introduction

Visual inspection of agricultural products plays a crucial role in postharvest supply chains. Traditionally, this process has relied heavily on manual inspection, which is labor-intensive, time-consuming, and prone to human error and inconsistency. The inspectors also need dedicated training, for example, to identify different defects, their size, and their severity. Typical defects for banana fruit are, for example, surface bruises and scars, insect damage, sunburn, chilling injuries, malformed fruits, or maturity stains. As a result, there has been a growing interest in leveraging advanced technologies such as computer vision and machine learning to enhance the accuracy and efficiency of visual inspection and grading of agricultural products (Yuvaraj et al., 2023; Barthwal et al., 2024). That way, inspectors with limited training could still accurately identify different defects and the severity of these defects in the field via a smartphone, which is very scalable, also to remote areas.

Machine learning-based computer vision models can establish an automated assessment procedure that increases the speed and consistency of grading. Traditionally, these AI models, however, require a considerably large and well-annotated training dataset to work well in real-life scenarios. However, large parts of the local, regional, and export postharvest supply chain are decentralized,

non-automated, and not digitalized from farm to retail. Therefore, stakeholders often do not have large annotated datasets readily available for their specific use case, defects, and cultivars that could be used to set up these AI models (De-Arteaga et al., 2018). Recent computer vision research shows a trend toward *foundation models* that are pre-trained on large (often unlabeled) datasets, enabled by advances in self-supervised learning (Balestriero et al., 2023). These models can be more easily adapted to complex downstream tasks by requiring less fine-tuning data compared to the previous generation of models and, therefore, facilitate the implementation of machine learning solutions in low data regimes (Knott et al., 2023). Most foundation models can be adapted to various tasks in a specific data modality (e.g., text, image, or time series) or across modalities (e.g., Li et al., 2024; Zhang et al., 2023). Other foundation models are designed to excel in a certain task or domain problem within a modality (e.g., Israel et al., 2023; Shah et al., 2023; Lu et al., 2024).

In this work, we aim to demonstrate that visual foundation models can be used to detect defects based on a relatively low number of images and with coarse annotations only. We address a common type of visual inspection: recognizing surface defects such as blemishes caused by external impacts (Abbas et al., 2019). Our study focuses on banana fruits and images taken via non-static cameras (e.g., smartphones) in the field and in sorting and packing facilities. We identified two key indicators relevant for grading: the *number* and *size* of blemishes visible on a bunch. In

*Corresponding author: thijs.defraeye@empa.ch

addition, the *type* of the defect is of secondary interest as it can help supply chain operators identify the cause of the defect. Such a use case is typically approached via *Image Segmentation*, a subcategory of Computer Vision that requires training data with dense image annotations, meaning each pixel has to be associated with a category and/or instance, traditionally leading to a tedious annotation process. To address this, our method utilizes the Segment Anything Model (SAM, Kirillov et al., 2023), a visual foundation model that specializes in image segmentation. We use SAM to generate dense image annotations from coarse high-level annotations (bounding boxes) and use them to train another image segmentation model that identifies, classifies, and segments banana surface defects in an image. We demonstrate that this method works well on a small dataset of 476 coarsely annotated images.

2. Materials and Methods

2.1. Data collection

We collected 476 images of single banana bunches containing at least one visible bruise or scar in three different sorting and packing facilities in India located in Tembhurni (Maharashtra state), Raver (Maharashtra state), and Kamrej (Gujarat state). The images were taken with different smartphone cameras between harvesting and packing. Due to the small dataset size, these images are split into five subsets used for cross-validation. This means that we evaluate all results on five different train-validation splits to ensure the robustness of our results. To ensure independent data samples, each bunch was only photographed once. The photos have realistic, non-standardized properties: the proximity to the fruits, lighting conditions, image sharpness, and resolution can vary. Also, there can be other bananas and objects occasionally in the background. Such conditions are typical for images taken in supply chains by inspectors, so we wanted our method to accommodate that. We aim to first automatically detect, segment, and classify defects using a machine learning model. In the second step, we derive the number of visible surface defects and their relative size from these predictions.

There are different principal approaches to defining target labels in image segmentation. One can assign each pixel to a general class (“semantic segmentation”) or to both a class and an instance (“instance segmentation”). The choice depends on the use case. This work uses a mixed approach called “panoptic segmentation”, which we will justify in the following paragraphs. See Section 2.2 for a more detailed explanation of the segmentation concepts.

Defect annotations. The images were then annotated by a single expert using the open-source tool “LabelStudio” (Tkachenko et al., 2020). As we are interested in the number of defects, we annotated defects on an instance level, meaning that we annotated one bounding box per defect.



Figure 1: **Defect examples.** Example images of banana surface defects we aim to detect in this study. Bruises usually result from a dull impact, while scars are caused due to a sharp impact. Old defects are usually darker than new defects as they oxidize over time.

While a key property of our approach is to only use bounding boxes and generate instance masks via SAM, we also annotate defect masks for validation purposes. Specifically, each defect was one of four categories: “Old Bruise”, “New Bruise”, “Old Scar”, and “New Scar”.

Bruises typically result from blunt force or pressure, which can arise from various factors such as handling, packing, impacts, or weight. Scars, on the other hand, are caused by sharp contact due to reasons like friction from leaves or stems, cuts from knives, crates, rough handling, laborers’ nails, or the sharp tips and crowns of neighboring bunches. Old defects are usually darker than new defects as they oxidize over time (see Figure 1). While the automated detection of generic defects without classification is already an impactful use case, we chose to add this categorization as it helps supply chain managers trace back the cause of the damage in the supply chain. It is important to note that there are cases that cannot be unambiguously assigned to one of those categories, even by expert annotators. However, a sub-goal of this work is to assess to which degree an automated classification is possible. It is worth mentioning that there are plenty of other relevant surface defects, reducing the quality of banana crops that are not included in this study, e.g., insect damage, speckles, sunburn, maturity stains, malformed fruits, broken necks, or chemical residues.

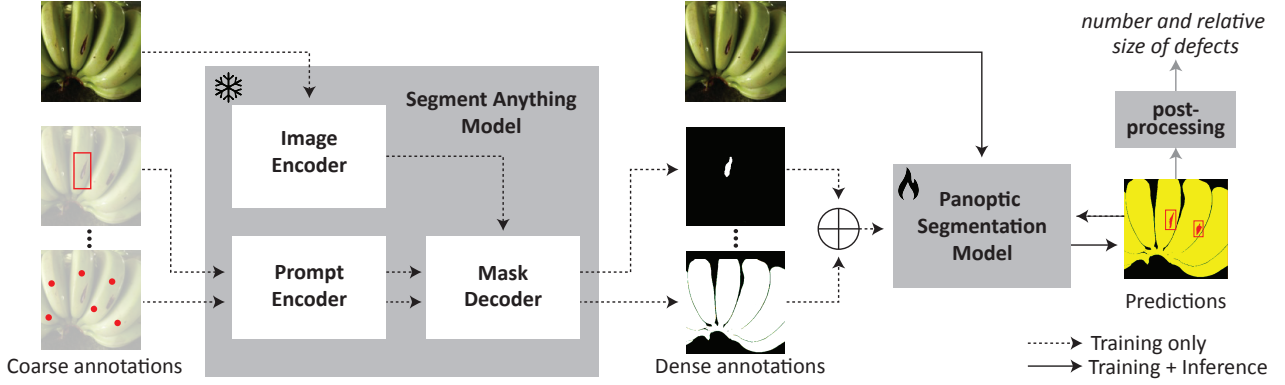


Figure 2: **Overview of our approach.** We utilize the Segment Anything Model (SAM), a promptable visual foundation model for image segmentation, to generate dense annotations (pixel-wise class and instance labels) from coarse annotations (bounding boxes and reference points) without any model training involved. These dense annotations otherwise require tedious hand-annotation. Using these newly generated labels, we train a panoptic segmentation model to identify surface defects on banana fruits, specifically bruises and scars. Additionally, the model can differentiate between foreground banana fruits and those in the background. This enables us to determine the number and size of visible surface defects from photographs of banana fruits. We validate our approach using a dataset of 476 images.

Banana annotations. To obtain relative defect sizes, we also annotated segmentation masks of banana fruits. We decided to only annotate bananas semantically on a pixel level, omitting instance information for two reasons: First, as images often contain multiple bunches that are partly cropped or occluded, it is challenging to differentiate instances. Second, our use case does not require us to identify instances, as we are not interested in counting single bananas or bunches. We would rather distinguish focused foreground bunches from those that may appear in the background and, therefore, annotate two types of pixel classes: “Foreground Banana” and “Background Banana”. All pixels not annotated as a banana of defect are assigned the “Background” class. We annotated banana masks using LabelStudio and Segment Anything point prompts (see Section 2.3 for more details).

2.2. Image segmentation

Image segmentation uses computer vision techniques to analyze and understand images on a pixel level. In this section, we describe different paradigms of image segmentation and their corresponding evaluation metrics that we use to evaluate the quality of our models.

2.2.1. Semantic Segmentation

“Semantic segmentation” is concerned with classifying each pixel of an image into a predefined category (e.g., background, banana fruit, defect) without distinguishing between individual objects (instances) of the same class. (Ronneberger et al., 2015; Chen et al., 2017; Xie et al., 2021)

Semantic segmentation maps are evaluated against a groundtruth using the Intersection-over-Union (IoU) score for a single class or the mean IoU (mIoU) score for all N classes in a dataset (Everingham et al., 2012; Lin et al., 2014). Eqs. 1 and 2 show the definition of those metrics where G refers to the set of groundtruth pixels that are

assigned to a class and P to the set of prediction pixels accordingly.

$$IoU(G, P) = \frac{|G \cap P|}{|G \cup P|} \quad (1)$$

$$mIoU = \frac{1}{N} \sum_{i=1}^N IoU_i \quad (2)$$

2.2.2. Instance Segmentation

Instance segmentation goes a step further by categorizing each pixel and identifying each object instance of the same class separately. This is realized by assigning each pixel to one of potentially multiple objects and to a semantic class simultaneously. This technique is essential for tasks requiring counting or differentiating between items. It is considered more complex, combining object detection with pixel classification. (He et al., 2017; Lin et al., 2017)

In terms of evaluation, instance segmentation is equivalent to object detection, which in machine learning describes the localization of instances via rectangular bounding boxes. The only difference is that the overlap of instances is defined by masks rather than boxes. There are several widely recognized metrics that compare a set of groundtruth bounding boxes or instance masks to a set of predicted bounding boxes or instance masks. Generally, a predicted and an annotated instance are matched if their localization exceeds a certain IoU threshold. As a first step, we calculate the precision P and recall R as follows:

$$P = \frac{TP}{TP + FP} \quad (3)$$

$$R = \frac{TP}{TP + FN} \quad (4)$$

where TP is the number of true positives, FP is the number of false positives, and FN is the number of false negatives. By definition, precision and recall are inversely

related but must concur effectively to ensure that both relevant and correct instances are identified. The primary evaluation metric for object detection is *Average Precision (AP)* for a single class and *mean Average Precision (mAP)* for multiple classes. We follow established practices and report three different variations:

- *AP@50*: *AP* at a *IoU* threshold of 0.50 as the most common metric in many benchmarks (e.g., Everingham et al., 2012),
- *AP@75*: *AP* at a *IoU* threshold of 0.75 as a more strict metric,
- *AP* (or *AP^{IoU=:.50:.05:.95}*): *AP* averaged over ten equidistant *IoU* thresholds between 0.50 and 0.95 as proposed by Lin et al. (2014).

The average recall is another evaluation metric used to measure the assertiveness of object detectors for a given class (Padilla et al., 2021). Similar to *AP*, the *AR* metric evaluates a range of IOU thresholds. We use the equation provided by Hosang et al. (2015) to calculate *AR* from a discrete set of thresholds based on the total number of ground truth instances G in an image:

$$AR = \frac{2}{G} \sum_{i=1}^G \max(IoU_i - 0.5, 0) \quad (5)$$

2.2.3. Panoptic Segmentation

In scenarios where one requires both instance-level information for some classes that are countable (widely referred to as “things”) and semantic information about other non-countable components (referred to as “stuff”), these two concepts need to be combined into an approach called “Panoptic Segmentation”. This approach seeks to overcome the limitations of its predecessors by delivering a comprehensive segmentation map that includes both class labels and instance identification. (Cheng et al., 2021, 2022; Kirillov et al., 2019a,b)

In our study, we declare defects as “things” and bananas as “stuff” as we are not interested in distinguishing single banana fruits. Thus, we simplify the machine learning task.

Kirillov et al. (2019b) propose *Panoptic Quality (PQ)* as a comprehensive metric for panoptic image segmentation (Eq. 6). The intuition behind *PQ* is to provide a unified measure that captures the accuracy of detecting and correctly segmenting individual objects (defects in our case) as well as the overall segmentation quality of the entire scene. *PQ* combines precision (how many predicted segments are correct) and recall (how many true segments are detected) into a single score, rewarding models that can accurately identify object boundaries and classify them correctly.

$$PQ = \frac{\sum_{(p,g) \in TP} IoU(p,g)}{|TP| + \frac{1}{2}|FP| + \frac{1}{2}|FN|} \quad (6)$$

In this work, we use Panoptic Quality as the primary evaluation metric to compare how well trained image segmentation models perform.

2.3. Segment Anything Model (SAM)

The Segment Anything Model (SAM) is a recently published foundation model for image segmentation (Kirillov et al., 2023). It was trained on a large-scale dataset comprising diverse images from various domains, including natural scenes, urban environments, medical imagery, and other contexts. It is the first model of its kind specifically tailored for generalized image segmentation and promises to facilitate the implementation of domain-specific segmentation models.

Figure 2 (left) shows a high-level overview of SAM’s components. The model consists of three major components: (1) a vision transformer (Dosovitskiy et al., 2020) pre-trained with the Masked Autoencoder method (He et al., 2021) that serves as an *image encoder*; (2) a prompt encoder that allows the user to specify bounding boxes or points to localize the region of interest in an image¹; (3) a mask decoder that generates segmentation masks based on the concatenated image and prompt embeddings. This approach yields impressive results for zero-shot instance segmentation in various domains. However, compared to conventional segmentation models, it comes with two disadvantages that require further adaptations or post-processing to enable SAM for a typical image segmentation use case: Firstly, SAM requires weak labels such as bounding boxes or point coordinates as input prompts. Secondly, the output masks are uncategorized, which hinders zero-shot usage of SAM in a multi-class setting.

SAM2 (Ravi et al., 2024) is a recent extension of SAM to the video domain. Although videos are not the focus of this work, SAM2 has demonstrated that their video-based pre-training enhances zero-shot mask generation for images as well. In our study, we assess both SAM and SAM2 using a ViT-L backbone for zero-shot mask generation of banana fruits and defects.

2.4. Experimental setup

Figure 2 shows an overview of our approach. The process starts with an image dataset with coarsely annotated labels: bounding boxes to locate and assign labels to defects and sets of points that identify foreground and background bananas. We utilize a promptable foundation model for image segmentation (SAM) to generate fine-grained pixel-wise annotations of each image in the dataset based on the coarse hand annotations. It is important to note that SAM is not trained in this procedure but is used here in a zero-shot manner to infer dense annotations only.

¹In their paper, the authors of SAM mention open vocabulary text as input prompts. However, they did not publish their code for this feature as the results are not as good as for other prompts (REF needed). Therefore, we do not consider this option in this research.

These newly created annotations are used to train a panoptic segmentation model in a standard supervised machine learning workflow. The panoptic segmentation model we use is a Maskformer (Cheng et al., 2021) model pre-trained on the ADE20k dataset (Zhou et al., 2017). Further details on model training, such as hyperparameters and data augmentation, can be found in Appendix A.

Cross-validation. Given the relatively small size of our training dataset, it is important to ensure that our reported results are robust. To achieve this, we use five-fold cross-validation instead of a static validation split. This approach involves dividing the dataset into five equally sized parts. We repeat each experiment five times, with one partition serving as the validation set while the remaining four partitions are used to train the model in each iteration. The evaluation metrics are then reported as the mean and standard deviation across these five experiments.

Validating SAM masks. Qualitative analysis indicated that SAM-generated defect masks are generally plausible. However, to quantify the impact of training on SAM-generated masks compared to using hand-annotated pixel-wise masks, we repeat our experiments with different combinations of mask sources for training and validation data: (a) both training and validation use hand-annotated defect masks; (b) both training and validation use SAM-generated defect masks; and (c) training uses SAM-generated masks while validation uses hand-annotated masks. By comparing the evaluation metrics across these three variations, we can quantify the trade-off between the time-saving benefits of automated mask generation and the quality of the resulting output.

2.5. Postprocessing

In some cases, it can be ambiguous whether to treat closely located defects as a single defect or multiple defects. To address this and ensure more consistent defect separation, we introduce a simple algorithm-based postprocessing method with the following three steps: (1) Combine all defect instances of the same type into a single binary map. (2) Use a connected components algorithm (OpenCV, 2015) to generate new instances where no pixels are connected. (3) Apply a dilation operation to expand all instance masks by d pixels (we choose $d = 5$) in all directions. This expanded auxiliary mask is then used to identify overlapping instances, which are subsequently merged. In other words, defect instances of the same class within a distance of $2d$ pixels are merged.

2.6. Deriving number and size of defects

In the context of quality estimation, we are interested in two practical indicators that can be derived from an image’s panoptic prediction: The *number* and *size* of defects. While the first can be estimated by counting the number of defect instances, an accurate metrical size estimation

in a two-dimensional image is impossible due to unknown scale and distortions. Thus, we use the *relative* defect size, simplified as the number of visible defect pixels divided by the number of visible foreground banana pixels, as a proxy.

3. Results and Discussion

3.1. Comparison of annotated and generated masks

Our approach uses SAM to generate dense segmentation masks in a zero-shot setting (i.e., without pre-training). To assess the quality of these masks, we first compare the masks produced by different SAM models (SAM and SAM2) with hand-annotated ground truth masks (Figure 3). Overall, we observe a high overlap between the hand-annotated defect masks and those generated by both SAM models. Notably, SAM2 exhibits even greater accuracy than SAM, with 90.5% of its masks achieving an IoU score of 0.5 or higher. Based on these findings, we conclude—and later demonstrate—that our zero-shot mask generation approach is both valid and capable of producing segmentation results comparable to hand-annotated masks.

3.2. Evaluation with image segmentation metrics

Next, we assess image segmentation results on validation images using the metrics outlined in Section 2.2. Table 1 presents these metrics across various experimental setups: In the first experiment, we used hand-annotated defect masks for both training and validation, achieving an average panoptic quality (PQ) of 77.5% after applying postprocessing. This serves as our baseline for assessing how segmentation quality changes when replacing hand-annotated masks with SAM-generated ones. In the second experiment, we employ SAM-generated masks for both training and validation. The results show comparable PQ scores of 77.3% (SAM) and 77.6% (SAM2). In the final experiment, SAM-generated masks are used for training, while hand-annotated masks are used for validation. Here, the PQ scores are approximately $\sim 0.5\%$ lower for both SAM and SAM2 compared to when hand-annotated masks are used for training. In conclusion, while SAM-generated masks are not fully equivalent to hand-annotated ones—occasionally failing to capture certain edge cases—they still produce metrics that are sufficiently close to be considered a viable low-effort alternative: For our dataset, we estimated an annotation time of approx. 15 seconds per image for coarse annotations and 3-5 minutes per image for pixel-wise annotations. An additional interpretation of these results is that there is a slight but consistent difference in how our human annotator and SAM delineate defect boundaries. Nonetheless, the Maskformer model demonstrates the ability to learn from both annotation styles effectively. Lastly, it is evident that our postprocessing method is effective for improving defect masks.

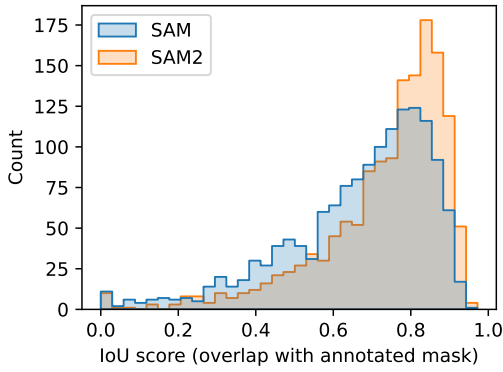


Figure 3: **Distribution of IoU values when comparing annotated and SAM-generated defect masks.** We generally observe a high overlap, while SAM2 masks are closer aligned to the hand-annotated ones.

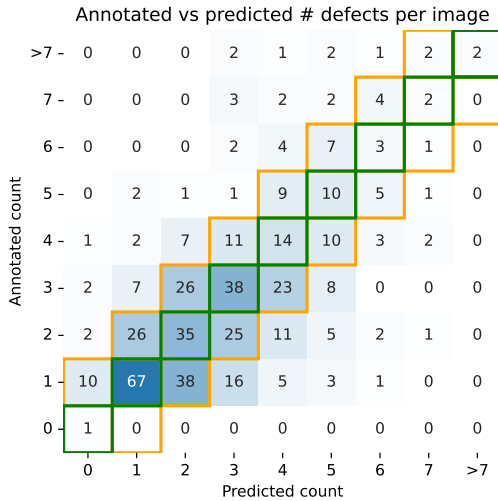


Figure 4: **Hand-annotated vs. estimated defect counts per image.** We predict the exact number of defects 36.5% of the time (green squares). 78.3% of the time, we predict correctly within a ± 1 tolerance (orange squares). Generally, our model tends to predict more defects in the images compared to the annotations.

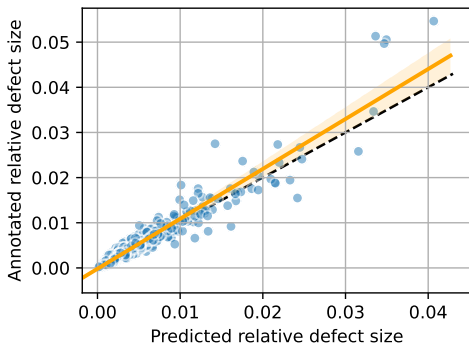


Figure 5: **Annotated vs estimated defect sizes.** We pairwise match those defect instances with the highest IoU agreement between annotation and estimation (minimum 0.5) and calculate their sizes relative to the corresponding foreground banana masks. Relative size prediction is generally accurate with a Pearson correlation of $r = 0.96, n = 829$. Each blue dot is one pair of defects, the orange line is a fitted regression line, black line is $x = y$ diagonal.

3.3. Qualitative evaluation

The results can be qualitatively analyzed through the example visualizations in Figure 6 showing the segmentation using a single generic defect class. In general, the masks appear sharp, particularly for bananas, and the model reliably distinguishes between fruits in the foreground or center of the image and those in the background. While the detected defects do not always align with the annotations, they are generally plausible. The model often identifies blemishes that were not annotated, likely because they were deemed too minor to be significant. This underscores the challenge of defining ground-truth defect annotations in these images.

3.4. Number and size of defects

Panoptic segmentation masks can simply be used to derive the number and size of defects. We compare the number of defects detected per image (Figure 4) and the relative defect sizes (Figure 5) by our best model (x-axes) and the human annotations (y-axes).

The model accurately matches the exact number of defects in 36.5% of cases and is off by one in 78.3% of cases. This further highlights the issue of ambiguous ground truth, as discussed earlier.

For relative size analysis, we pairwise match those defect instances with the highest IoU agreement between annotation and estimation. If no agreement with at least 0.5 IoU can be established, we consider predicted defects non-matchable and exclude them from this analysis. Relative sizes are calculated by dividing the number of pixels of a specific defect instance by the aggregated number of pixels assigned to either the foreground banana class or any defect. We generally see a high agreement in predicted vs. annotated relative sizes ($r = 0.96$), while the model tends to slightly underestimate sizes, visible by the different slopes of the regression line (orange) and $x = y$ (black dashed) lines in Figure 5.

3.5. Defect Categorization

We also conducted experiments using four distinct defect types instead of a single defect class (see Appendix B for details). In this setup, the model must not only detect and segment defects but also categorize them into one of four pre-defined classes. Our results clearly show that while the detection and segmentation of bruises and scars work well, a reliable categorization into one of the four predefined classes is not possible with the current approach and dataset. We hypothesize that this limitation stems from one or more of the following factors:

1. Ambiguous annotation: The classification of defects across the four predefined categories may be subjective to a large degree. The distinction between “old” and “new” defects is not always clear-cut, as the transition is gradual. Additionally, distinguishing bruises from scars can be ambiguous, especially for non-experts (see Figure 1).

Table 1: **Main results with a single defect category.** All results are reported via their mean and standard deviation over the five different cross-validation splits. We compare different setups where target defect masks are either annotated (“Anno.”) or generated by SAM/SAM2. Expectedly, when Maskformer is trained on SAM-generated masks, the defect IoU is slightly lower when evaluating annotated masks. However, recall and precision are comparable to the fully annotated setting. We also demonstrate that our postprocessing (“PP”) significantly improves precision and recall of defects. Banana segmentation quality is slightly better in the fully annotated setting (~ 0.81 vs ~ 0.80 mIoU). The configuration highlighted in blue is used for subsequent visualizations.

Model	PP	Defect masks		Defects					Fruits		Overall	
		train	val	AP	AP@50	AP@75	AR	IoU	IoU FG	IoU BG	mIoU	PQ
Maskformer		Anno.	Anno.	.133 ± .022	.243 ± .027	.134 ± .027	.256 ± .036	.593 ± .032	.952 ± .005	.732 ± .034	.812 ± .010	.758 ± .010
Maskformer	✓	Anno.	Anno.	.220 ± .019	.422 ± .014	.215 ± .033	.412 ± .041	.593 ± .032	.952 ± .005	.732 ± .034	.813 ± .010	.775 ± .007
Maskformer		SAM	Anno.	.128 ± .030	.234 ± .043	.128 ± .040	.238 ± .025	.546 ± .040	.951 ± .006	.731 ± .052	.800 ± .011	.752 ± .011
Maskformer	✓	SAM	Anno.	.205 ± .017	.392 ± .040	.197 ± .013	.380 ± .022	.548 ± .039	.951 ± .006	.731 ± .052	.801 ± .011	.770 ± .005
Maskformer		SAM	SAM	.137 ± .030	.241 ± .045	.141 ± .034	.250 ± .027	.561 ± .038	.951 ± .006	.731 ± .052	.804 ± .012	.755 ± .010
Maskformer	✓	SAM	SAM	.220 ± .016	.404 ± .044	.222 ± .016	.399 ± .023	.562 ± .037	.951 ± .006	.731 ± .052	.804 ± .011	.773 ± .005
Maskformer		SAM2	Anno.	.121 ± .028	.227 ± .047	.121 ± .036	.238 ± .034	.555 ± .025	.950 ± .005	.720 ± .041	.799 ± .015	.753 ± .011
Maskformer	✓	SAM2	Anno.	.201 ± .022	.395 ± .018	.184 ± .030	.392 ± .020	.554 ± .025	.950 ± .005	.720 ± .041	.799 ± .015	.770 ± .013
Maskformer		SAM2	SAM2	.134 ± .039	.229 ± .050	.139 ± .054	.249 ± .044	.579 ± .028	.950 ± .005	.720 ± .041	.805 ± .015	.757 ± .012
Maskformer	✓	SAM2	SAM2	.225 ± .035	.405 ± .029	.221 ± .056	.415 ± .034	.579 ± .028	.950 ± .005	.720 ± .041	.805 ± .015	.776 ± .012

- Image resolution: We use 1024^2 pixel resolution for images. While this is generally considered high for machine learning tasks, defects can be small and, thus, only be represented by a few pixels, making them harder to categorize.
- The four defect types are unevenly represented in our dataset (37/82/387/834). A more balanced distribution of categories and a larger number of defect samples are likely to improve categorization accuracy. We recommend collecting more examples from the two underrepresented classes for future work.

4. Conclusion and Outlook

In this work, our objective was to have an efficient way to implement machine learning to count the number of defects on banana fruit and have their relative sizes. We demonstrated the use of a panoptic image segmentation model to tackle the detection and pixel-wise segmentation of bananas and surface blemishes in images. Our approach significantly reduces the effort required for hand annotation by relying on coarse labels. Specifically, we utilize a pre-trained foundation model for image segmentation (the Segment Anything Model) to generate the dense annotations necessary for training the panoptic model. This method reduces the manual annotation workload by at least a factor of 10 while maintaining high-quality results: the measured Panoptic Quality drops from 77.5% to 77.0%) w.r.t. the annotated targets.

Our results generally demonstrate reliable and plausible segmentation of both foreground and background bananas, as well as a single generic defect category. However, when compared to human annotations, the model matches the exact number of defects in only 36.5% of cases and is off by up to one defect in 78.3% of cases. While some of this discrepancy can be attributed to model performance, it is more likely due to the target annotations. Unlike

for other machine learning applications where target labels are often close to a “ground truth”, the identification of *significant* blemishes is to a certain degree subjective. An improvement on the labeling side could be to employ multiple annotators and measure their level of agreement. The benefits of using (noisy) annotations from multiple annotators for samples that are non-trivial to label have been explored in the machine learning literature (Welinder et al., 2010; Sheng et al., 2008). Thus, we recommend that future work carries out a more sophisticated annotation process with multiple expert annotators. The disagreement between annotators could then serve as a baseline for evaluating the performance of future machine learning models.

In addition, we demonstrated that with our current method and dataset, it is not possible to reliably categorize defects into one of the four predefined classes, namely new scars, old scars, new bruises, and old bruises. A variable ground truth is likely a contributing factor, along with the skewed class distribution and the potentially low image resolution for small defect sizes. Addressing these challenges will require further investigation in future work to improve the reliability of defect categorization.

Our method demonstrates the potential for dense image segmentation in low-data scenarios and can be broadly applied to any commodity with countable, localizable defects. However, for defects that are non-countable—such as speckles, sunburn, or chemical residues—a different machine learning paradigm (such as classification) would be more applicable.

Acknowledgments

This work was partially funded by the project “Scaling up Your Virtual Cold Chain Assistant”, commissioned by the German Federal Ministry of Economic Cooperation and Development (BMZ) on behalf of the German International Cooperation Agency (GIZ).

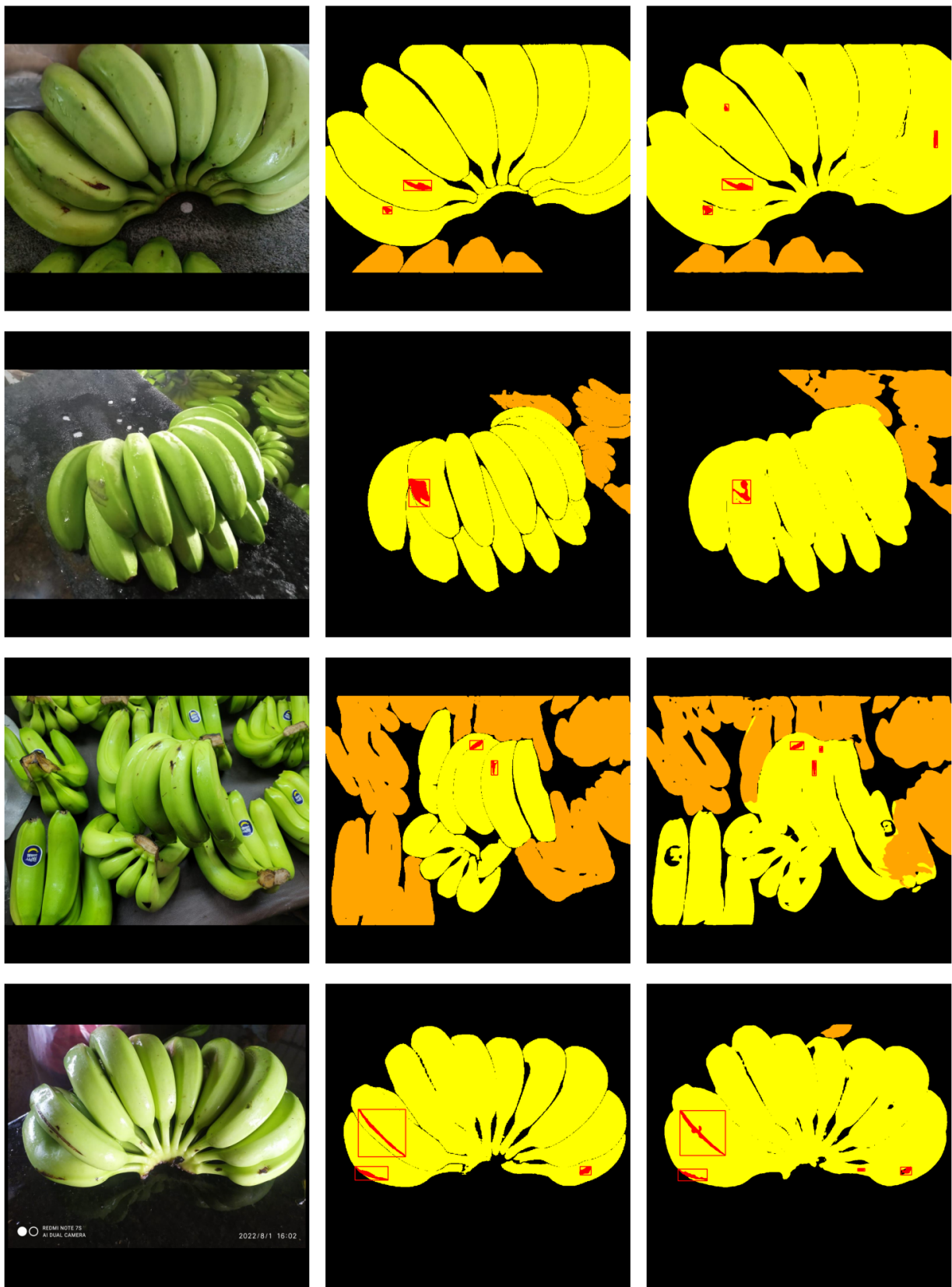


Figure 6: **Example visualizations of annotated vs predicted masks using a single defect category.** Left: Input Image, Mid: Annotation (SAM), Right: Maskformer Prediction. Segments are color-coded as follows: **Foreground Banana**, **Background Banana**, **Defect**.

Supplementary materials

The source code of all experiments, as well as pre-trained models, can be accessed on GitHub: <https://github.com/manuelknott/banana-defect-segmentation>.

References

- Abbas, H.M.T., Shakoor, U., Khan, M.J., Ahmed, M., Khurshid, K., 2019. Automated sorting and grading of agricultural products based on image processing, in: Proceedings of the 2019 8th International Conference on Information and Communication Technologies (ICICT), Institute of Electrical and Electronics Engineers Inc.. pp. 78–81. doi:10.1109/ICICT47744.2019.9001971.
- Balestriero, R., Ibrahim, M., Sobal, V., Morcos, A., Shekhar, S., Goldstein, T., Bordes, F., Bardes, A., Mialon, G., Tian, Y., Schwarzschild, A., Wilson, A.G., Geiping, J., Garrido, Q., Fernandez, P., Bar, A., Pirsiavash, H., LeCun, Y., Goldblum, M., 2023. A Cookbook of Self-Supervised Learning. arXiv preprint arXiv:2304.12210 .
- Barthwal, R., Kathuria, D., Joshi, S., Kaler, R., Singh, N., 2024. New trends in the development and application of artificial intelligence in food processing. *Innovative Food Science & Emerging Technologies* , 103600 Publisher: Elsevier.
- Chen, L.C., Papandreou, G., Schroff, F., Adam, H., 2017. Rethinking atrous convolution for semantic image segmentation. arXiv preprint arXiv:1706.05587 .
- Cheng, B., Misra, I., Schwing, A.G., Kirillov, A., Girdhar, R., 2022. Masked-attention Mask Transformer for Universal Image Segmentation, in: CVPR.
- Cheng, B., Schwing, A.G., Kirillov, A., 2021. Per-Pixel Classification is Not All You Need for Semantic Segmentation, in: NeurIPS.
- De-Arteaga, M., Herlands, W., Neill, D.B., Dubrawski, A., 2018. Machine Learning for the Developing World. *ACM Transactions on Management Information Systems* 9, 1–14. doi:10.1145/3210548.
- Dosovitskiy, A., Beyer, L., Kolesnikov, A., Weissenborn, D., Zhai, X., Unterthiner, T., Dehghani, M., Minderer, M., Heigold, G., Gelly, S., Uszkoreit, J., Houshy, N., 2020. An Image is Worth 16x16 Words: Transformers for Image Recognition at Scale. arXiv preprint doi:10.48550/arXiv.2010.11929.
- Everingham, M., Van Gool, L., Williams, C.K.I., Winn, J., Zisserman, A., 2012. The PASCAL Visual Object Classes Challenge 2012 (VOC2012). URL: <http://www.pascal-network.org/challenges/VOC/voc2012/workshop/index.html>.
- He, K., Chen, X., Xie, S., Li, Y., Dollár, P., Girshick, R.B., 2021. Masked Autoencoders Are Scalable Vision Learners. 2021 IEEE/CVF Conference on Computer Vision and Pattern Recognition (CVPR) , 15979–15988.
- He, K., Gkioxari, G., Dollár, P., Girshick, R., 2017. Mask R-CNN, in: Proceedings of the IEEE International Conference on Computer Vision, pp. 2961–2969.
- Hosang, J., Benenson, R., Dollár, P., Schiele, B., 2015. What makes for effective detection proposals? *IEEE transactions on pattern analysis and machine intelligence* 38, 814–830. Publisher: IEEE.
- Israel, U., Marks, M., Dilip, R., Li, Q., Yu, C., Laubscher, E., Li, S., Schwartz, M., Pradhan, E., Ates, A., others, 2023. A foundation model for cell segmentation. bioRxiv Publisher: Cold Spring Harbor Laboratory Preprints.
- Kingma, D.P., 2014. Adam: A method for stochastic optimization. arXiv preprint arXiv:1412.6980 .
- Kirillov, A., Girshick, R., He, K., Dollár, P., 2019a. Panoptic feature pyramid networks, in: Proceedings of the IEEE/CVF conference on computer vision and pattern recognition, pp. 6399–6408.
- Kirillov, A., He, K., Girshick, R., Rother, C., Dollár, P., 2019b. Panoptic segmentation, in: Proceedings of the IEEE/CVF conference on computer vision and pattern recognition, pp. 9404–9413.
- Kirillov, A., Mintun, E., Ravi, N., Mao, H., Rolland, C., Gustafson, L., Xiao, T., Whitehead, S., Berg, A.C., Lo, W.Y., Dollár, P., Girshick, R., 2023. Segment Anything. arXiv:2304.02643 .
- Knott, M., Perez-Cruz, F., Defraeye, T., 2023. Facilitated machine learning for image-based fruit quality assessment. *Journal of Food Engineering* 345, 111401. URL: <https://linkinghub.elsevier.com/retrieve/pii/S0260877422004551>, doi:10.1016/j.jfoodeng.2022.111401.
- Li, C., Gan, Z., Yang, Z., Yang, J., Li, L., Wang, L., Gao, J., others, 2024. Multimodal foundation models: From specialists to general-purpose assistants. *Foundations and Trends in Computer Graphics and Vision* 16, 1–214. Publisher: Now Publishers, Inc.
- Lin, T.Y., Dollár, P., Girshick, R., He, K., Hariharan, B., Belongie, S., 2017. Feature pyramid networks for object detection, in: Proceedings of the IEEE conference on computer vision and pattern recognition, pp. 2117–2125.
- Lin, T.Y., Maire, M., Belongie, S., Hays, J., Perona, P., Ramanan, D., Dollár, P., Zitnick, C.L., 2014. Microsoft coco: Common objects in context, in: *Computer Vision—ECCV 2014: 13th European Conference, Zurich, Switzerland, September 6–12, 2014, Proceedings, Part V 13*, Springer. pp. 740–755.
- Lu, M.Y., Chen, B., Williamson, D.F., Chen, R.J., Liang, I., Ding, T., Jaume, G., Odintsov, I., Le, L.P., Gerber, G., others, 2024. A visual-language foundation model for computational pathology. *Nature Medicine* 30, 863–874. Publisher: Nature Publishing Group US New York.
- OpenCV, 2015. Open Source Computer Vision Library.
- Padilla, R., Passos, W.L., Dias, T.L., Netto, S.L., Da Silva, E.A., 2021. A comparative analysis of object detection metrics with a companion open-source toolkit. *Electronics* 10, 279. Publisher: MDPI.
- Ravi, N., Gabeur, V., Hu, Y.T., Hu, R., Ryali, C., Ma, T., Khedr, H., Rädle, R., Rolland, C., Gustafson, L., others, 2024. Sam 2: Segment anything in images and videos. arXiv preprint arXiv:2408.00714 .
- Ronneberger, O., Fischer, P., Brox, T., 2015. U-Net: Convolutional Networks for Biomedical Image Segmentation, in: Navab, N., Hornegger, J., Wells, W.M., Frangi, A.F. (Eds.), *Medical Image Computing and Computer-Assisted Intervention – MICCAI 2015*. Springer International Publishing, Cham. volume 9351, pp. 234–241.
- Shah, D., Sridhar, A., Dashora, N., Stachowicz, K., Black, K., Hirose, N., Levine, S., 2023. Vint: A foundation model for visual navigation. arXiv preprint arXiv:2306.14846 .
- Sheng, V.S., Provost, F., Ipeirotis, P.G., 2008. Get another label? improving data quality and data mining using multiple, noisy labels, in: Proceedings of the 14th ACM SIGKDD international conference on Knowledge discovery and data mining, pp. 614–622.
- Tkachenko, M., Malyuk, M., Holmanyuk, A., Liubimov, N., 2020. Label Studio: Data labeling software. URL: <https://github.com/heartexlabs/label-studio>.
- Welinder, P., Branson, S., Perona, P., Belongie, S., 2010. The multidimensional wisdom of crowds. *Advances in neural information processing systems* 23.
- Xie, E., Wang, W., Yu, Z., Anandkumar, A., Alvarez, J.M., Luo, P., 2021. SegFormer: Simple and efficient design for semantic segmentation with transformers. *Advances in Neural Information Processing Systems* 34, 12077–12090.
- Yuvaraj, M., Jothi Basu, R., Abdulrahman, M.D.A., Ganesh Kumar, C., 2023. Implementation of information and communication technologies in fruit and vegetable supply chain: a systematic literature review. *Industrial Management & Data Systems* 123, 2349–2377. Publisher: Emerald Publishing Limited.
- Zhang, J., Zhou, Z., Mai, G., Mu, L., Hu, M., Li, S., 2023. Text2seg: Remote sensing image semantic segmentation via text-guided visual foundation models. arXiv preprint arXiv:2304.10597 .
- Zhou, B., Zhao, H., Puig, X., Fidler, S., Barriuso, A., Torrallba, A., 2017. Scene Parsing through ADE20K Dataset. 2017 IEEE Conference on Computer Vision and Pattern Recognition (CVPR) , 5122–5130.

Supplementary Materials

Appendix A. Implementation details

All images were resized and padded to 1024^2 pixels resolution. Training images were augmented with a 50% Random Horizontal Flip and with additional random color-based augmentations (see Table A.1) to increase model robustness.

Table A.2 shows the hyperparameters used for training the Maskformer models. We evaluated the model every five epochs on the validation set and saved the model with the highest Panoptic Quality. All trainings were done on a single NVIDIA RTX A5000 GPU with 24GB memory.

Table A.1: **Random color augmentations applied to training images.** Values are uniformly sampled from the specified ranges.

Property	Sampling range
brightness	[0.9, 1.1]
contrast	[0.9, 1.1]
saturation	[0.9, 1.1]
hue	[-0.05, 0.05]

Table A.2: **Hyperparameters for Maskformer training.**

Batch size	2
Epochs	100
Evaluation frequency	every 5 epochs
Optimizer	Adam (Kingma, 2014)
Learning rate	5×10^{-5}
Learning rate schedule	constant

Appendix B. Results using four defect categories

Table B.3: **Results using multiple defect categories.** It is evident that our models are unable to categorize defect types. Most likely due to ambiguous annotations and/or limited training data. The configuration highlighted in [blue](#) is used for the visualizations in Figure B.1.

Model	PP	Defects										Overall		
		Defect masks		Old Bruise		New Bruise		Old Scar		New Scar		mAP	mIoU	PQ
		train	val	AP	IoU	AP	IoU	AP	IoU	AP	IoU			
Maskformer		Anno.	Anno.	.027 ± .060	.011 ± .024	.058 ± .024	.186 ± .107	.039 ± .035	.229 ± .048	.063 ± .026	.376 ± .077	.047 ± .020	.493 ± .018	.471 ± .013
Maskformer	✓	Anno.	Anno.	.009 ± .020	.051 ± .061	.063 ± .013	.115 ± .067	.030 ± .021	.199 ± .062	.034 ± .013	.123 ± .061	.034 ± .009	.447 ± .028	.442 ± .021
Maskformer		SAM	Anno.	.000 ± .000	.000 ± .000	.058 ± .031	.166 ± .078	.031 ± .019	.243 ± .038	.064 ± .035	.351 ± .067	.038 ± .014	.488 ± .012	.462 ± .008
Maskformer	✓	SAM	Anno.	.000 ± .000	.003 ± .006	.071 ± .024	.079 ± .046	.024 ± .018	.178 ± .055	.040 ± .014	.122 ± .035	.034 ± .010	.433 ± .014	.440 ± .007
Maskformer		SAM	SAM	.000 ± .000	.000 ± .000	.061 ± .034	.173 ± .081	.035 ± .020	.247 ± .042	.069 ± .036	.359 ± .067	.041 ± .014	.490 ± .013	.467 ± .007
Maskformer	✓	SAM	SAM	.000 ± .000	.000 ± .001	.077 ± .026	.083 ± .049	.029 ± .024	.180 ± .058	.043 ± .014	.125 ± .036	.037 ± .010	.434 ± .016	.442 ± .006
Maskformer		SAM2	Anno.	.000 ± .000	.000 ± .000	.047 ± .019	.144 ± .082	.039 ± .038	.235 ± .086	.062 ± .014	.394 ± .052	.037 ± .007	.490 ± .021	.467 ± .009
Maskformer	✓	SAM2	Anno.	.000 ± .000	.021 ± .031	.064 ± .033	.127 ± .083	.027 ± .019	.168 ± .064	.033 ± .012	.094 ± .038	.031 ± .007	.437 ± .017	.437 ± .017
Maskformer		SAM2	SAM2	.000 ± .000	.000 ± .000	.049 ± .019	.152 ± .086	.055 ± .065	.242 ± .090	.067 ± .012	.405 ± .053	.043 ± .014	.494 ± .022	.472 ± .011
Maskformer	✓	SAM2	SAM2	.000 ± .000	.020 ± .030	.067 ± .036	.133 ± .086	.038 ± .034	.170 ± .066	.036 ± .013	.098 ± .039	.035 ± .003	.439 ± .018	.442 ± .019

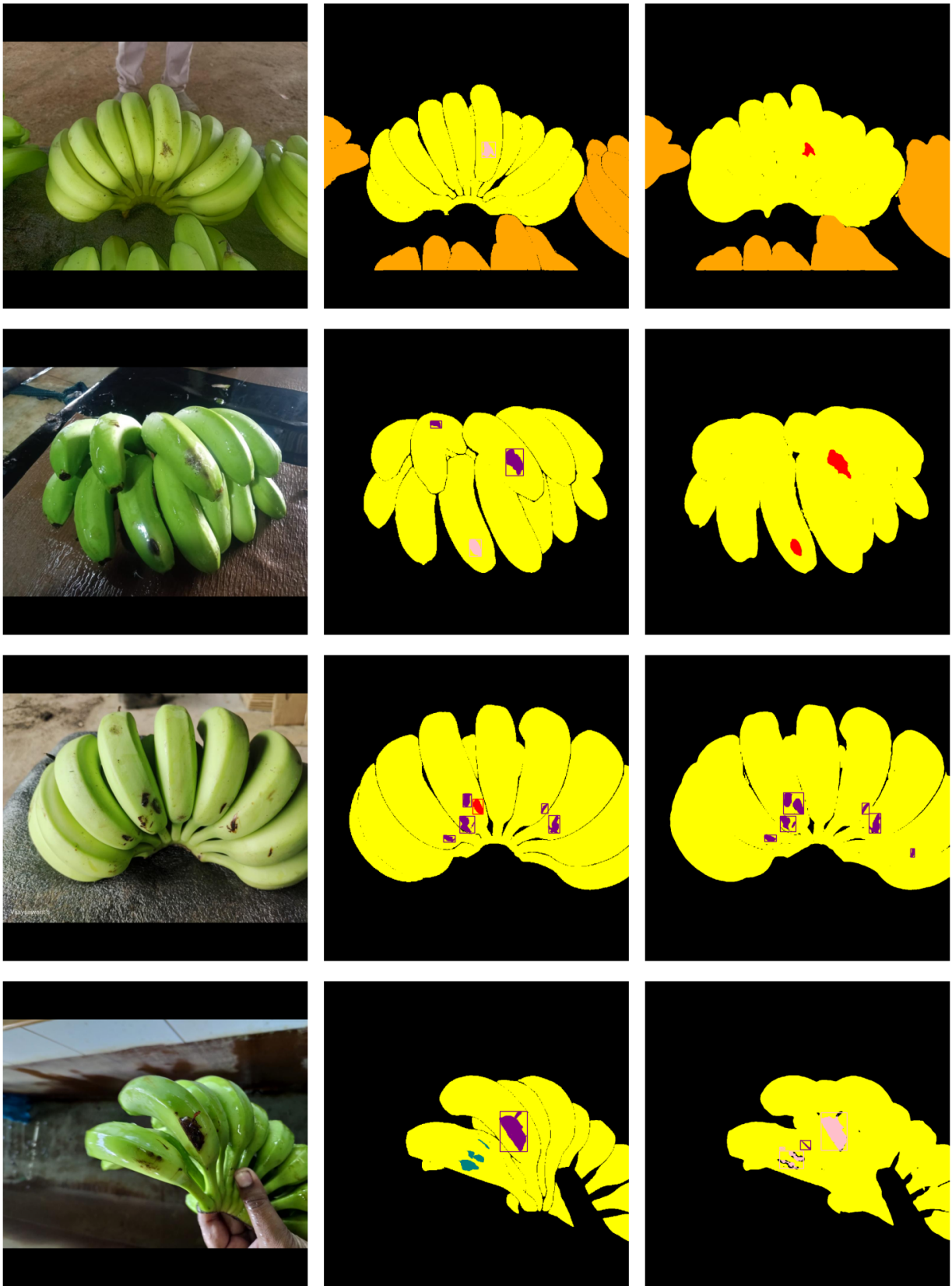


Figure B.1: **Example visualizations of annotated vs. predicted masks using four defect categories.** Left: Input Image, Mid: Annotation, Right: Maskformer Predictions (SAM2). Segments are color-coded as follows: **Foreground Banana**, **Background Banana**, **Old Bruise**, **Old Scar**, **New Bruise**, **New Scar**.